

Functional Amyloids in *Pseudomonas aeruginosa* Are Essential for the Proteome Modulation That Leads to Pathoadaptation in Pulmonary Niches

Beg, Ayesha Z.; Rashid, Faraz; Talat, Absar; Haseen, Mohd Azam; Raza, Nadeem; Akhtar, Kafil; Dueholm, Morten Kam Dahl; Khan, Asad U.

Published in:
Microbiology Spectrum

DOI (link to publication from Publisher):
[10.1128/spectrum.03071-22](https://doi.org/10.1128/spectrum.03071-22)

Creative Commons License
CC BY 4.0

Publication date:
2023

Document Version
Publisher's PDF, also known as Version of record

[Link to publication from Aalborg University](#)

Citation for published version (APA):

Beg, A. Z., Rashid, F., Talat, A., Haseen, M. A., Raza, N., Akhtar, K., Dueholm, M. K. D., & Khan, A. U. (2023). Functional Amyloids in *Pseudomonas aeruginosa* Are Essential for the Proteome Modulation That Leads to Pathoadaptation in Pulmonary Niches. *Microbiology Spectrum*, 11(1), Article e03071-22. <https://doi.org/10.1128/spectrum.03071-22>

General rights

Copyright and moral rights for the publications made accessible in the public portal are retained by the authors and/or other copyright owners and it is a condition of accessing publications that users recognise and abide by the legal requirements associated with these rights.



- Users may download and print one copy of any publication from the public portal for the purpose of private study or research.
- You may not further distribute the material or use it for any profit-making activity or commercial gain
- You may freely distribute the URL identifying the publication in the public portal -

Take down policy

If you believe that this document breaches copyright please contact us at vbn@aub.aau.dk providing details, and we will remove access to the work immediately and investigate your claim.



Functional Amyloids in *Pseudomonas aeruginosa* Are Essential for the Proteome Modulation That Leads to Pathoadaptation in Pulmonary Niches

Ayesha Z. Beg,^a Faraz Rashid,^b Absar Talat,^a Mohd Azam Haseen,^c Nadeem Raza,^d Kafil Akhtar,^e  Morten Kam Dahl Dueholm,^f  Asad U. Khan^a

^aMedical Microbiology Lab, Interdisciplinary Biotechnology Unit, Aligarh Muslim University, Aligarh, Uttar Pradesh, India

^bHenry Ford Health System Detroit, Michigan, USA

^cDepartment of Cardiothoracic Surgery, Jawaharlal Nehru Medical College, Aligarh Muslim University, Aligarh, Uttar Pradesh, India

^dDepartment of Anaesthesiology, Jawaharlal Nehru Medical College, Aligarh Muslim University, Aligarh, Uttar Pradesh, India

^ePathology Department, Jawaharlal Nehru Medical College, Aligarh Muslim University, Aligarh, Uttar Pradesh, India

^fCenter for Microbial Communities, Department of Chemistry and Bioscience, Aalborg University, Aalborg, Denmark

ABSTRACT Persistence and survival of *Pseudomonas aeruginosa* in chronic lung infections is closely linked to the biofilm lifestyle. One biofilm component, functional amyloid of *P. aeruginosa* (Fap), imparts structural adaptations for biofilms; however, the role of Fap in pathogenesis is still unclear. Conservation of the *fap* operon encoding Fap and *P. aeruginosa* being an opportunistic pathogen of lung infections prompted us to explore its role in lung infection. We found that Fap is essential for establishment of lung infection in rats, as its genetic exclusion led to mild focal infection with quick resolution. Moreover, without an underlying cystic fibrosis (CF) genetic disorder, overexpression of Fap reproduced the CF pathotype. The molecular basis of Fap-mediated pulmonary adaptation was explored through surface-associated proteomics *in vitro*. Differential proteomics positively associated Fap expression with activation of known proteins related to pulmonary pathoadaptation, attachment, and biofilm fitness. The aggregative bacterial phenotype in the pulmonary niche correlated with Fap-influenced activation of biofilm sustainability regulators and stress response regulators that favored persistence-mediated establishment of pulmonary infection. Fap overexpression upregulated proteins that are abundant in the proteome of *P. aeruginosa* in colonizing CF lungs. Planktonic lifestyle, defects in anaerobic pathway, and neutrophilic evasion were key factors in the absence of Fap that impaired establishment of infection. We concluded that Fap is essential for cellular equilibration to establish pulmonary infection. Amyloid-induced bacterial aggregation subverted the immune response, leading to chronic infection by collaterally damaging tissue and reinforcing bacterial persistence.

IMPORTANCE *Pseudomonas aeruginosa* is inextricably linked with chronic lung infections. In this study, the well-conserved Fap operon was found to be essential for pathoadaptation in pulmonary infection in a rat lung model. Moreover, the presence of Fap increased pathogenesis and biofilm sustainability by modulating bacterial physiology. Hence, a pathoadaptive role of Fap in pulmonary infections can be exploited for clinical application by targeting amyloids. Furthermore, genetic conservation and extracellular exposure of Fap make it a commendable target for such interventions.

KEYWORDS Fap, *Pseudomonas aeruginosa*, amyloid, antimicrobial resistance, biofilms

Pseudomonas aeruginosa is a multidrug-resistant bacterium associated with morbidity and mortality of patients with opportunistic nosocomial infections (1–3). *P. aeruginosa* frequently causes chronic lung infections, chronic wound infections, and medical device-facilitated infections (2, 4, 5). *P. aeruginosa* is inseparably linked with cystic fibrosis (CF), a

Editor Cezar M. Khursigara, University of Guelph

Copyright © 2022 Beg et al. This is an open-access article distributed under the terms of the [Creative Commons Attribution 4.0 International license](https://creativecommons.org/licenses/by/4.0/).

Address correspondence to Asad U. Khan, asadukhan72@gmail.com, or akhan.cb@amu.ac.in.

The authors declare no conflict of interest.

Received 5 August 2022

Accepted 14 November 2022

Published 8 December 2022

life-shortening genetic disorder characterized by mucus-mediated pulmonary obstruction and changes in lung architecture (6). Reportedly, almost three out of four adults with CF and approximately 98% of young CF patients are predominantly infected by *P. aeruginosa* (7). In the long run, aggressive antibiotic regimens fail to eradicate *Pseudomonas* colonization of CF lungs due to its persistent lifestyle in chronic infections (8). The premises of *P. aeruginosa* survival in CF lungs depends on host-pathogen interactions, where biofilm lifestyle obscures bacterial clearance by immune cells (9). Furthermore, biofilms impede the neutrophil-mediated response and generate a hyperinflammatory cycle, which leads to development of chronic infection (10).

Recent evidence has shown the biofilm lifestyle or aggregative phenotype is predominantly found in chronic pulmonary infections (11). The extracellular polymeric substance matrix impairs the response of the immune system and effectiveness of antibiotic regimens. The aforementioned scenario has directed a focus toward exploring targets involved in biofilm-mediated pathoadaptation (12). A biofilm is an adherent meshwork comprising exopolysaccharides, extracellular DNA, proteins (e.g., lectins, adhesins, and amyloids), and lipids (13–15). One of the biofilm components produced by *P. aeruginosa* is the Fap amyloids, which provide hydrophobicity and mechanical robustness to the biofilm (16). Fap also serves as a reservoir for retaining quorum-sensing molecules (17). Moreover, bioinformatic analysis of sequenced strain genomes has revealed that the Fap system is conserved in many genera and is present in almost all *P. aeruginosa* strains (18–20). Recent evidence associated other bacterial amyloids with pathologies associated with cognitive function, inflammatory responses, and pulmonary functions (21–24). However, similar effects have not been explored for Fap amyloids.

The known effects of Fap on biofilm properties, in combination with the conservation and sophisticated assembly of the *fap* genes into an operon, prompted us to explore its essentiality in pathoadaptation by *P. aeruginosa* (16, 17, 19). The *P. aeruginosa* PAO1 wild-type strain (PAO1 wt), a Fap deletion strain (PAO1 Δfap), and a Fap overexpression strain (PAO1 pFap) derivative were studied in a rat model of lung infection to infer the role of Fap-mediated adaptation in establishment of lung infection. An *in vivo* lung infection model was used to describe the effect of Fap on infection pathophysiology and host immune response. The molecular basis of Fap-mediated adaptations associated with attachment and biofilm sustainability were explored by *in vitro* surface-associated proteomics using a glass wool model (25, 26). The glass wool model was used to mimic the lung environment, as it provides a low-shear environment, with interstrand cellular movement and interchange of nutrients and oxygen (25, 26). Although the current *in vitro* biofilm models are limited by the absence of host factors, they are suitable for helping in understanding bacterial physiology. Surface-associated proteomics provided insight into Fap expression-influenced regulation of previously known pathoadaptive and cellular fitness proteins that account for generation of histopathology.

RESULTS

Effects of PAO1 Fap variants on biofilm formation and human whole blood. The relative biofilm quantification by a crystal violet (CV) assay showed highest biofilm formation by PAO1 pFap, followed by PAO1 wt and finally PAO1 Δfap (Fig. 1A). The hemolytic assay results were positively correlated with biofilm formation ability, demonstrating highest hemolysis by PAO1 pFap, followed by PAO1 wt and then PAO1 Δfap (Fig. 1B). The human whole-blood (HWB) assay demonstrated a slight difference in the numbers of polymorphonuclear leukocytes (PMNs), lymphocytes, and eosinophils (Fig. 1C), but a distinct infection profile was observed (Fig. 1D to G). The HWB infected by bacteria showed persistence of aggregated colonies for PAO1 pFap (marked bacteremia [score of 3+]) (Fig. 1E), PAO1 wt (moderate bacteremia [2+]) (Fig. 1F), and PAO1 Δfap (mild bacteremia [–]) (Fig. 1G).

Effects of Fap system in *in vivo* rat lung bacterial colonization. The implication of Fap in generation of lung infection was explored using *in vivo* rat models (Fig. 2). The PAO1 wt, PAO1 Δfap , and PAO1 pFap variants were inoculated into the lungs of rats through tracheostomy, and bacterial colonization and the progression of infection through histopathology were observed on days 3, 7, and 11.

Hematoxylin and eosin (H&E)-stained lung tissue sections were analyzed to visualize bacterial colonization. The rat groups exposed to PAO1 wt displayed dispersed bacteria

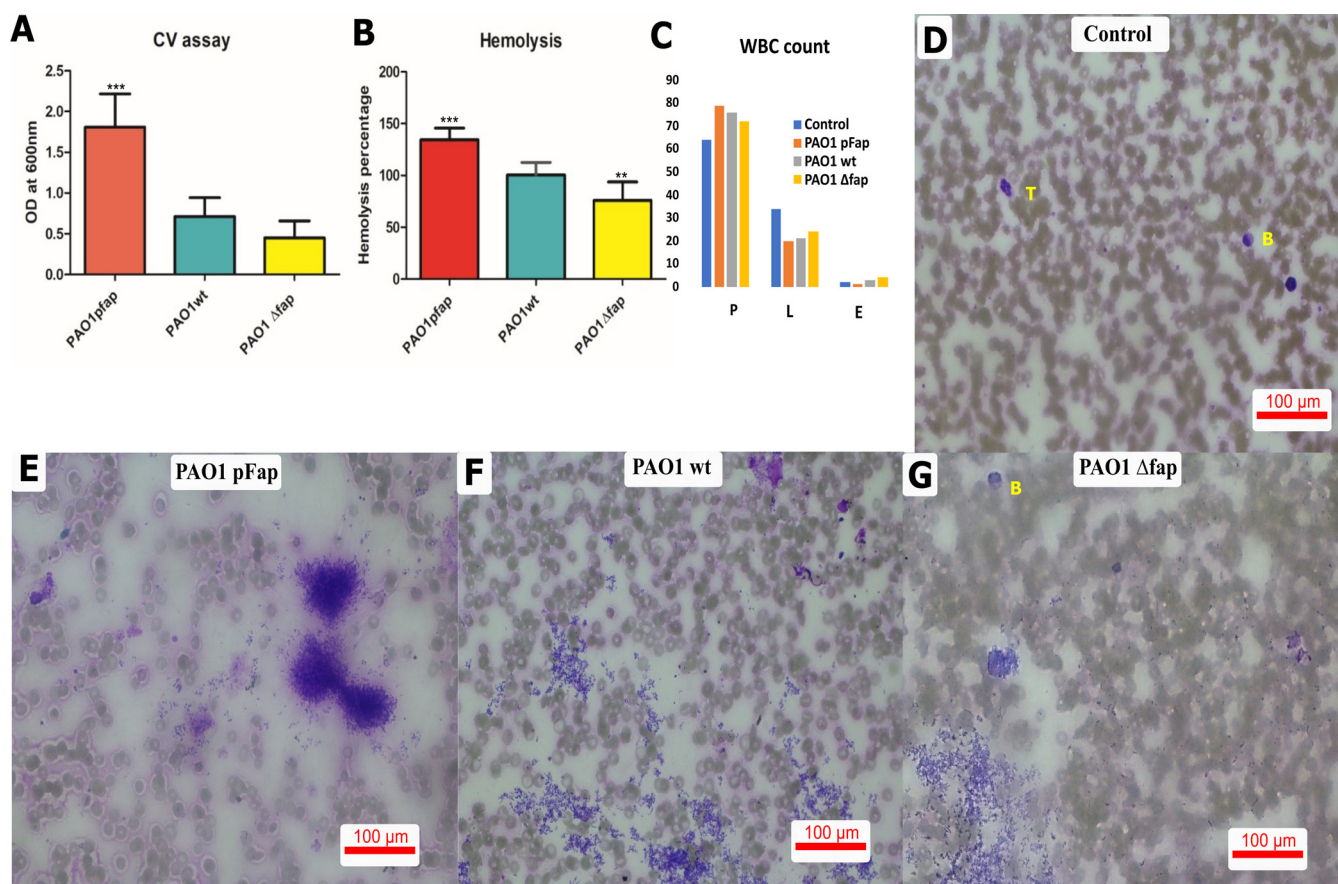


FIG 1 *In vitro* biofilm formation and pathogen-blood studies. (A) Relative quantification of biofilm formation in the CV assay indicated that pFap showed significant biofilm formation with respect to wt, and the group with Fap deleted showed decreased biofilm formation. (B) Hemolysis profiles of different Fap groups. (C) White blood cell (WBC) counts of different groups. P, polymorphonuclear leukocytes (PMN); L, lymphocytes; E, eosinophils. Significant hemolysis was observed in the pFap and Δ fap groups compared to the wild type. Other images show the peripheral blood smear of HWB infected with *P. aeruginosa* fap variants. (D) The control image shows bilobed (B) and trilobed (T) PMNs and red blood cells. (E) For PAO1 pFap, PMNs showed moderate (2+) to intense (3+) bacteremia; (F) PAO1 wt, the image shows PMN leukocytosis and moderate (2+) bacteremia; (G) PAO1 Δ fap, bilobed leukocytes (B) were evident with mild to moderate bacteremia. The assay results were subjected to a one-way ANOVA and are presented as means \pm SD.

and few bacterial aggregates (Fig. 3B), while exposure to PAO1 pFap led to aggregated bacterial colonization resembling a meshwork (Fig. 3C) compared to the control (Fig. 3A). However, fewer localized bacteria in alveolar space were observed in the PAO1 Δ fap group (Fig. 3D). After 11 days, bacterial load in the lung tissue indicated a chronic infection for PAO1 pFap, with 10^9 CFU/g of tissue. The bacterial load for PAO1 wt was 10^7 CFU/g of tissue, while 10^5 CFU/g of tissue PAO1 Δ fap bacterial load was determined (Fig. 3E). To confirm that the improved colonization was related to the expression of amyloid, lung tissues were stained with the amyloid-specific dyes Congo red (CR) and Thioflavin T (ThT). The combination of CR and ThT dyes was selected for amyloid confirmation, as CR staining produced background fluorescence of the tissues. The lung tissue sections colonized with PAO1 wt displayed dispersed amyloid deposits (Fig. 3I to K), while PAO1 pFap showed presence of dense amyloid deposits (Fig. 3L to N). Amyloids were not detected in the infection negative control (Fig. 3F to H) or in lungs infected with PAO1 Δ fap (Fig. 3O to Q).

Effects of Fap on infection pathology of lungs and cytokine response. (i)

Histopathological analysis. The H&E-stained lung tissue sections were analyzed, and pathology was graded as described in Materials and Methods. The control group lung sections from days 3, 7, and 11 demonstrated normal lung tissues (Fig. 4A to C). At day 3, the PAO1 wt-infected group showed mild alveolar dilation, vascular congestion, dense moderate neutrophilic aggregates, and peribronchial neutrophilic infiltrates (Fig. 4D). On day 7, peribronchial neutrophil infiltration increased along with bronchial hyperplasia and marked alveolar inflammation (Fig. 4E). At day 11, moderate congestion with marked interstitial inflammation and

In vivo rat lung infection model

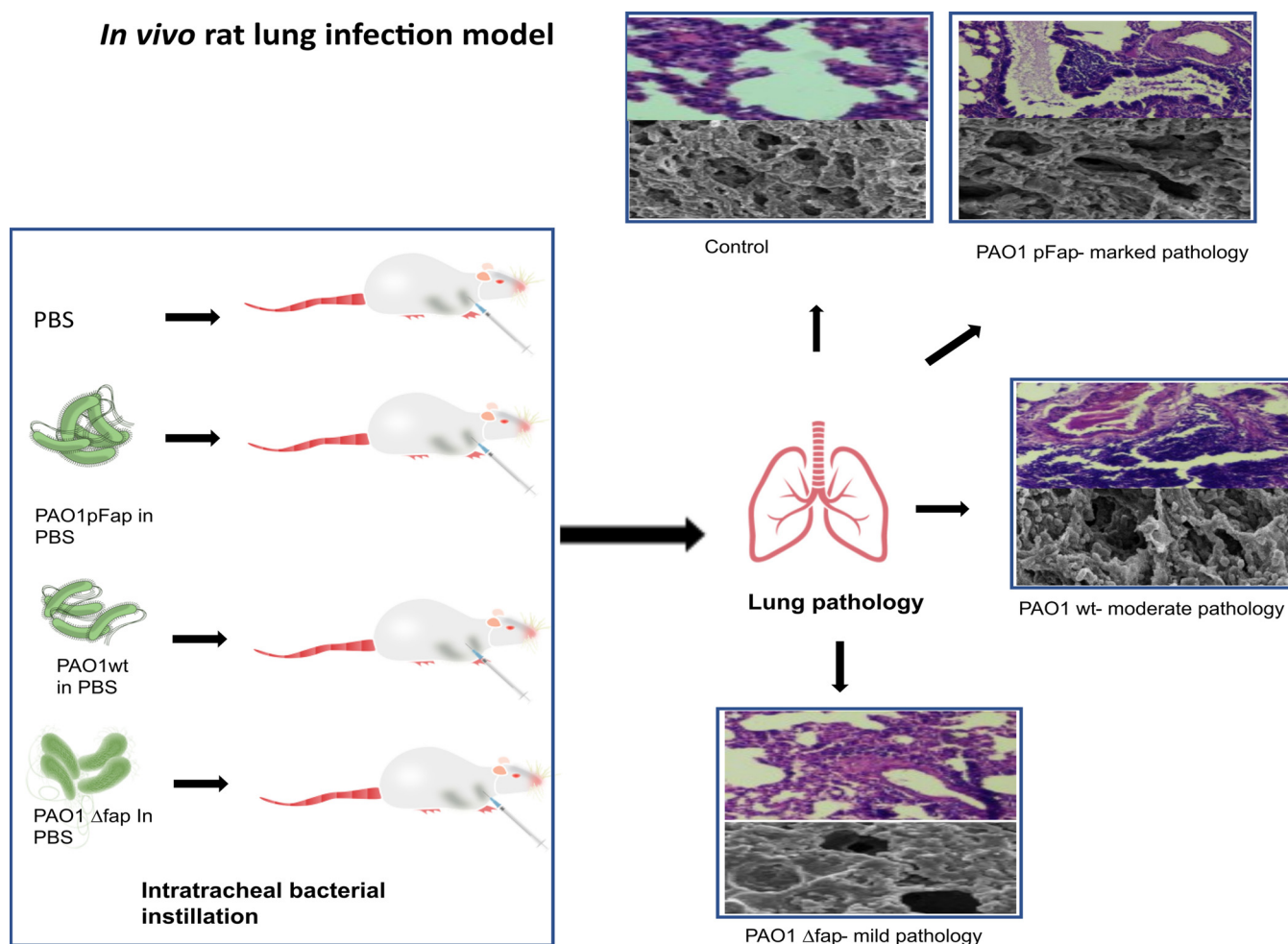


FIG 2 Schematic workflow for the rat lung infection model. (Left) Intratracheal bacterial instillation of different Fap variants in Wistar rats. (Right) Histopathological studies to determine infection progression.

bronchial epithelium destruction were observed (Fig. 4F). The infection progression pattern of the PAO1 pFap-infected group on day 3 displayed marked neutrophilic infiltration accompanied by inflammation, vascular congestion, and moderate alveolar dilation (Fig. 4G). On day 7, apart from persistent neutrophilic inflammation, characteristic emphysema with alveolar and bronchial destruction (27) and CF-like secretion in bronchial spaces were observed (Fig. 4H). On day 11, apart from chronic neutrophilic inflammation, persistent emphysema, increased alveolar dilation and edema, bronchiectasis with bronchial dilation, and CF-like secretion were also apparent (6) (Fig. 4I). The infection progression of the PAO1 Δ fap-infected group on day 3 showed mildly dilated bronchi and alveoli with focal neutrophilic infiltrates (Fig. 4J). Focal neutrophilic infiltration with mild acute peribronchial inflammation was observed on day 7 (Fig. 4K). Mild focal pathologies, like vascular congestion, neutrophilic infiltrates, and peribronchial inflammation, persisted until day 11 (Fig. 4L).

(ii) Ultrastructure of infected lungs. The ultrastructure of lung tissues was assessed by scanning electron microscopy (SEM), where the lung structure of the control group remained normal during the course of experiment (Fig. 5A and B). At day 3, slight narrowing of the alveolar lumen was observed in the PAO1 wt-infected group, which was complemented by fewer acanthocytes on day 7 (Fig. 5C). Narrowed air spaces and poikilocytes persisted until day 11 (Fig. 5D). On day 3, unusual narrowing of the alveolar lumen was observed in the PAO1 pFap-infected group, with an additional surge of acanthocytes on day 7 (Fig. 5E and F) (28). The collapsed alveolar spaces and poikilocytes persisted on day 11 with coalesced alveoli generating large airway lumen spaces (Fig. 5G). There were no

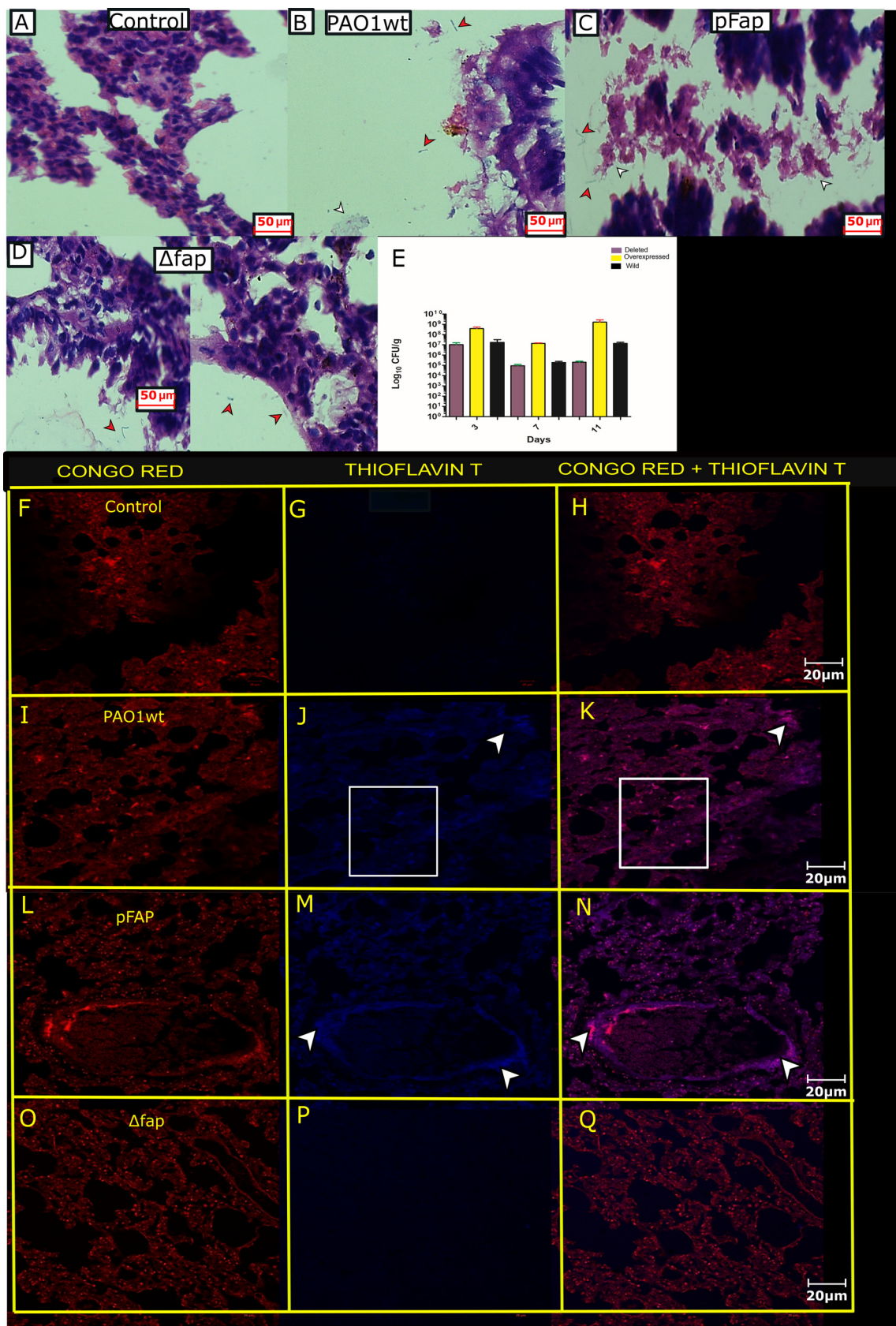


FIG 3 Bacterial colonization and detection of amyloid produced by bacteria in tissue sections. (A) Control H&E-stained lung tissue. (B) Lung tissue infected with the wild type as dispersed bacteria (red arrows) and aggregated form (white arrows) were visualized. (Continued on next page)

distinct changes observable with respect to the control in the PAO1 Δfap -infected group during the time course (Fig. 5H and I).

(iii) Inflammatory response of infection. Serum cytokine levels of interleukin-6 (IL-6), gamma interferon (IFN- γ), tumor necrosis factor alpha (TNF- α), and IL-1 β were assessed in all groups. Increases in IL-1 β are correlated with neutrophilic hyperinflammation in chronic infection (10). The IL-1 β sera levels in the PAO1 pFap group increased with progression of time compared to other groups (Fig. 5J). The IL-6, IFN- γ , and TNF- α levels in sera were found to be undetectable (29).

Surface-associated proteomics demonstrated the influence of Fap on bacterial adaptivity and fitness. The effects of the Fap system on the bacterial physiology associated with biofilm sustainability, pathoadaptivity, and cellular fitness were studied through surface-associated proteomics that could provide a link to the pulmonary histopathology. The differential protein expression patterns arising due to bacterial phenotypic heterogeneity were captured by surface-associated proteomics of two groups, the biofilm group and the surface-influenced planktonics (SIP) group (25). The grouping was done as follows: the biofilm group included PAO1 pFap versus PAO1 wt and PAO1 Δfap versus PAO1 wt; the SIP group included PAO1 pFap versus PAO1 wt and PAO1 Δfap versus PAO1 wt. The different proteomes in the absence and presence of a Fap system showed activation and suppression of critical interactomes involved in biofilm formation and maintenance, anaerobiosis, metabolic competency, cellular integrity, and fitness in protein machinery. Distinct expression of critical interactive domains in PAO1 pFap versus PAO1 wt and PAO1 Δfap versus PAO1 wt groups are illustrated in Fig. 6A and B. The comparisons of the PAO1 pFap versus PAO1 wt and PAO1 Δfap versus PAO1 wt nonoverlapping proteomes revealed 159 and 113 proteins, respectively, which were enriched in gene ontology (GO) classes (Fig. 6C). The GO classes associated with DNA metabolism, transcription machinery, and ATP-utilizing proteins were exclusive to PAO1 pFap versus PAO1 wt, indicating dynamism in regulatory circuits (Fig. 6C).

The SEM images of characteristic biofilm and morphologies of SIP cells of Fap variants subjected to proteomics are shown in Fig. 7A and B and provided correlation with expression of proteins and cellular morphologies. The differential expression of selective proteins that are relevant to pathoadaptation are shown in Fig. 7C to E, and a model elucidating their mechanism in adaptation is presented in Fig. 7F. Furthermore, differentially expressed proteins that demonstrated the linkage between Fap expression with proteome supporting biofilm lifestyles and adaptation to various stresses and the connection of absence of Fap with proteome sustaining planktonic lifestyle with lower cell fitness are discussed in detail below.

Cellular attachment, biofilm formation, and sustainability. The Fap-influenced proteins responsible for cellular attachment and biofilm development and maintenance are explained in detail in Fig. 7A and C. Transcription factor DksA (PA4273), a critical part of the bacterial stress response (SR GO category) which regulates quorum sensing (QS GO category), virulence, swarming, and biofilm formation, was upregulated in PAO1 pFap attached cells while downregulated in PAO1 Δfap SIP (30). DksA and GreA functionally competed to bind to RNA polymerase and modulate the transcription differently (30). GreA was upregulated in PAO1 Δfap SIP, while reciprocal expression was observed in PAO1 pFap SIP.

The T4P responsible for initial attachment and twitching-mediated biofilm expansion was significantly downregulated in PAO1 Δfap SIP (31, 32). The twitching-mediated biofilm expanders Pfpl (protease important for survival in reactive oxygen species [ROS]-rich chronic infection niche), FabF1 (beta-ketoacyl-acyl carrier protein synthase II), and FliM

FIG 3 Legend (Continued)

(C) Lung tissue infected with pfap. Bacteria are seen in the aggregated mesh (white arrows) and free form (red arrows). (D) Lung tissue infected with *fap*-deleted bacteria found localized in alveolar space (red arrows). (E) CFU per gram of lung for the different variants along the timeline of the experiments. (F) Control Congo red-stained lung tissue. (G) ThT-stained tissue. (H) Overlapped Congo red and ThT stain. (I) Lung tissue of the wild type stained with Congo red. (J) Arrow and box representing dense and dispersed amyloid deposits. (K) Overlapped stains (pink) showing amyloid deposits, indicate by the box and arrow. (L) Congo red-stained overexpressed infected tissue. (M) ThT-stained tissue section, where the arrow indicates fluorescence by amyloid deposits. (N) Overlap of both stains (pink) showing presence of amyloid deposits. (O) Deleted Fap variant, Congo red stained. (P) ThT stained. (Q) Overlapped stains showed absence of amyloid. Magnification: $\times 40$ (A to D) or $\times 20$ (F to Q). Note: CR staining produced background fluorescence of the tissue; therefore, amyloid confirmation was done in combination with ThT.

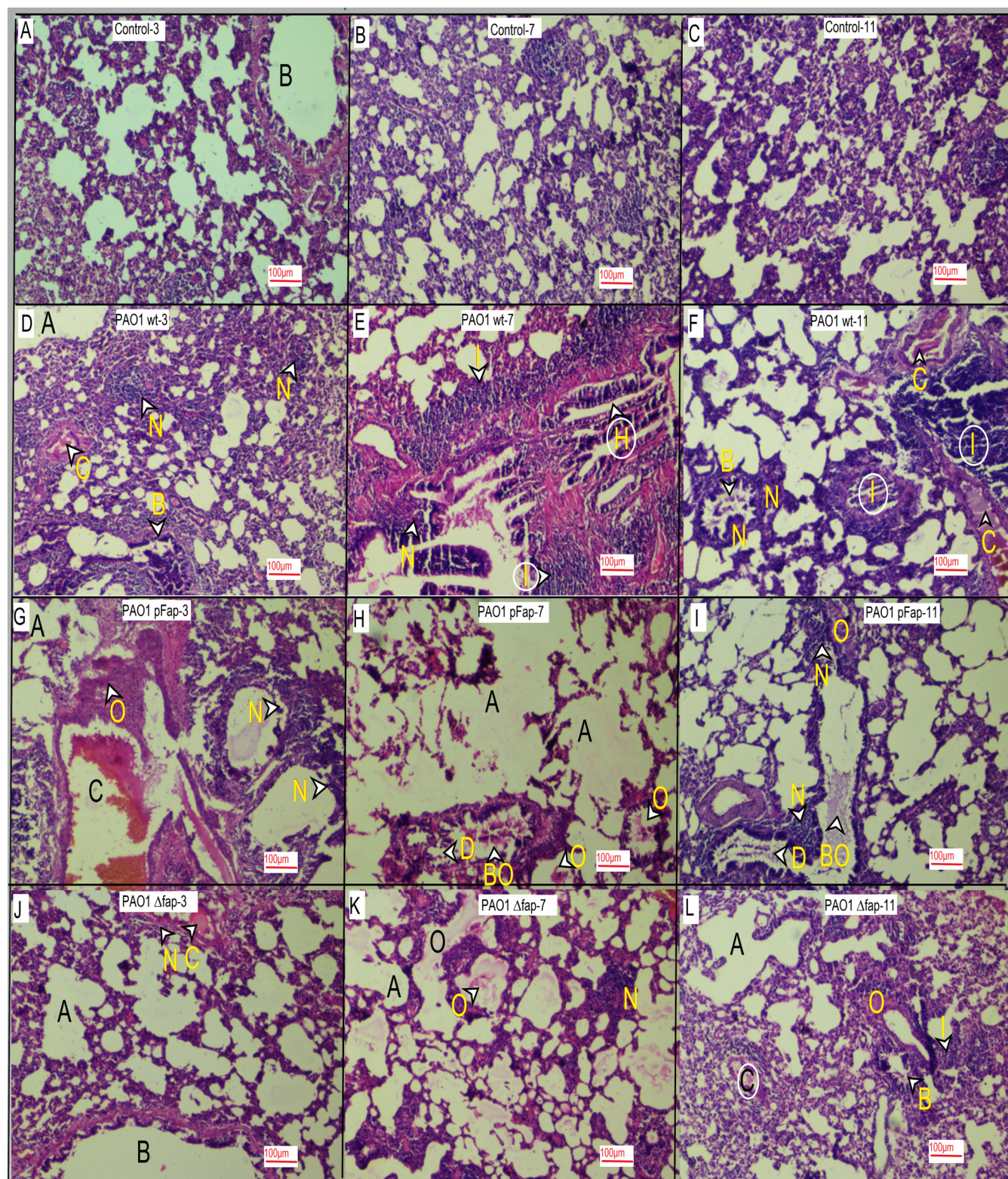


FIG 4 Histopathological analysis of lung tissues. (A) Control, day 3. Tissue section shows normal alveolar spaces and a bronchiole with normal stratified columnar epithelium with thin muscle layer. (B) Control, day 7. Tissue sections show normal alveolar spaces with normal capillaries in the alveolar septum. (C) Control, day 11. Tissue sections show normal alveolar spaces with normal capillaries in the alveolar septum. (D) Wild type, day 3. Section shows mildly (+) dilated alveoli (A), mild vascular congestion (C), dense moderate (2+) neutrophilic aggregates (N), and moderate (2+) bronchial neutrophilic infiltrate (B). (E) Wild type, day 7. Tissue sections show mild (+) dilated alveoli (A), marked (3+) dense peribronchial neutrophilic infiltrate (N), marked (3+) alveolar inflammation (I), and bronchial epithelial hyperplasia. (F) Wild type, day 11. Section shows mildly (+) dilated alveoli (A), moderate vascular congestion (C), marked (3+) interstitial inflammation (I), bronchial epithelium destruction (B), and mild peribronchial neutrophilic infiltrate (N). (G) Overexpressed *fap*, day 3. (Continued on next page)

were upregulated in the PAO1 pFap SIP group (31, 33, 34). The SIP state of PAO1 pFap displayed upregulated sensor-regulator hybrid SagS (PA2824), which promotes surface attachment by activating the motile-sessile switch through small RNA regulation and biofilm sustainability (35). Similarly, PqsB of PqsABCDE, whose production is central to stationary phase and promotion of biofilm formation, was significantly downregulated in PAO1 Δfap SIP (36).

Likewise, other miscellaneous proteins that affected biofilm sustainability were differentially expressed. The PAO1 Δfap SIP displayed significant upregulation of Dsps, an enoyl-coenzyme A hydratase or isomerase. Dsps is critical for swarming motility and biofilm dispersion but reciprocal to biofilm density (37). Another regulator, SuhB, inversely regulates biofilm formation under the influence of c-di-GMP through the Rsm/Gac pathway (38). In PAO1 Δfap SIP, SuhB was upregulated, but in the other group SuhB was downregulated. There was significant downregulation of stringent starvation protein A (SspA) in the PAO1 Δfap SIP group; this protein provides adaptation to stringent stress responses in a new environment (39). A nudix pyrophosphatase (PA5176) relieved ROS generation and also contributed toward motility and pathogenicity (40). PA5176 was found to be upregulated ~8-fold in PAO1 pFap attached cells. The PAO1 pFap attached cells displayed upregulation of survival protein E (SurE), which facilitates survival of cells in stationary phase (41).

Metabolism-mediated cellular fitness and adaptation. The PAO1 Δfap SIP displayed significant suppression of DksA, Anr, and a nitrite reductase (NIR) protein involved in anaerobic respiration during oxygen stress in lungs (Fig. 7D). Apart from being essential for biofilm in an anaerobic state, NIR genes maintained the elongated cell morphology that causes effective cellular clumping leading to robust biofilm formation (Fig. 7B) (42). The suppression in proteins associated with anaerobiosis in PAO1 Δfap SIP explained the rod-shaped cellular morphology (Fig. 7B) (42). The PAO1 wt and PAO1 pFap strains displayed elongated cellular morphology (Fig. 7B), which were supported by a functional anaerobic pathway (42).

PAO1 pFap biofilm showed upregulation of glucose-6-phosphate 1-dehydrogenase (Zwf), phosphoglycerate kinase (Pgk), enolase (Eno), and PA3190, which are associated with glycolytic metabolism (Fig. 7D). Zwf provides fitness in the CF environment and sputum and prevents growth inhibition of *Pseudomonas* (43), while enolase is critical for lung colonization and osmoprotection (44). Pgk provides ROS-induced metabolic fitness (45), while PA3190 is responsible for the glucose uptake operon (46). A stress response regulator, OxyR, was downregulated in Δfap SIP; this regulator is required for establishing infection and evasion of neutrophils (47) (Fig. 7D).

Fatty acid metabolism, cellular membrane, and chaperones. The PAO1 Δfap SIP displayed downregulation of multiple proteins associated with synthesis and metabolism of fatty acids and cellular wall components like OprL of Tol-Pal and FabD, AccB, PA3013, and HisF2 (Fig. 7E). The OprL of the Tol-Pal system is involved in biogenesis of the outer membrane, assembly of porins, and transfer of lipopolysaccharides (48). AccB under the influence of SigX maintains the cell envelope integrity (49). FabA is involved in fatty acid metabolism, and PA3013 and HisF2 are associated with lipopolysaccharide biosynthesis (50–52). The “CF-selected proteins” Fab, Acc, and OprL, which facilitate integrity-mediated fitness in the CF lung environment, were upregulated in PAO1 pFap (53). Attached PAO1 pFap showed upregulation of FabF1, which is responsible for appendages and membrane fluidity, and KdsC, which is essential for liposaccharide production responsible for cellular integrity (54, 55). A protease, PA3611, was 10-fold upregulated in PAO1 pFap biofilm, which is associated with lung inflammation and bronchial fibrosis (56). Another CF-select OmpA to -C-like protein

FIG 4 Legend (Continued)

Section shows moderately (2+) dilated alveoli (A), marked (3+) vascular congestion (C), marked (3+) peribronchial neutrophilic infiltrate (N), interstitial inflammation (I), and alveolar edema (O). (H) Overexpressed *fap*, day 7. Section shows marked (3+) alveolar destruction and dilation (A) turning into alveolar sacs with alveolar edema (O), bronchial destruction (D), and bronchial edema (BO). (I) Overexpressed *fap*, day 11. Section shows moderately (2+) to markedly (3+) dilated alveoli (A), alveolar edema (O), bronchial destruction (D), edema (BO), and focal marked (3+) neutrophilic infiltrate around bronchi (N). (J) Deleted *fap*, day 3. Tissue section shows mildly (+) dilated alveoli, focal neutrophilic infiltrate (N), mild (+) vascular congestion (C), and mildly (+) dilated bronchi (B). (K) Deleted *fap*, day 7. Section shows mildly (+) to moderately (2+) dilated alveoli (A), alveolar edema (O), mild peribronchial acute inflammation (B) (I), and mild (+) focal interstitial neutrophilic infiltrate (N). (L) Deleted *fap*, day 11. Section shows mildly dilated (+) alveoli (A), mild (+) vascular congestion (C), interstitial edema (O), mild (+) interstitial neutrophilic infiltrate (I), and mild (+) peribronchial inflammation (B). Magnification (all images), $\times 10$.

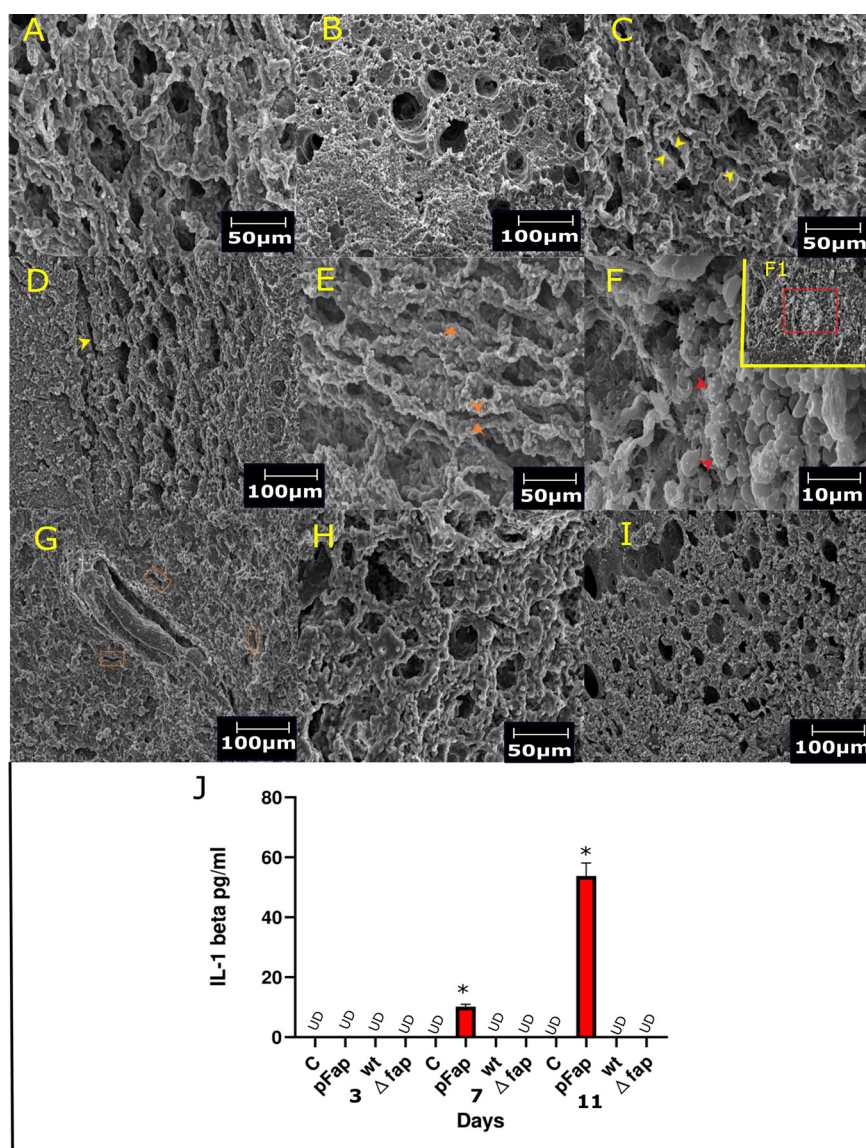


FIG 5 Ultrastructure of lung tissue and systemic levels of cytokines. (A) Day 3, control: normal alveolar space was observed. (B) Day 11, control: normal lung architecture. (C) Day 3, PAO1 wt: changes in airway architecture (yellow arrows). (D) Day 11, PAO1 wt: moderate narrowing of alveolar lumen (yellow arrow). (E) Day 3, PAO1 pFap: extensive alveolar space collapse (orange arrows). (F) Day 7, PAO1 pFap: influx of acanthocytes (red arrow), F1 broader view demonstrating marked presence of acanthocytes (red box). (G) Day 11, PAO1 pFap: marked collapse and obstruction of airways (orange boxes). (H) Day 3, Fap deleted: no prominent observation was apparent. (I) Day 11, Fap deleted: in comparison with control, no significant observation was made. (J) Cytokine panel, for IL-1 β measured for different groups at a certain time point, significant change was observed in the Fap overexpressed group on day 11, while it remained undetectable (UD) in other groups. Magnification: $\times 500$ (A to D, day 3 lung sections); $\times 2,500$ (E, day 7 pFap); $\times 200$ (F to I, day 11 lung sections). Cytokine assays were performed in technical duplicates. Significance and nonsignificance (ns) were determined with respect to PAO1 wt. *, $P < 0.01$.

(PAO833) was upregulated in PAO1 pFap biofilm; this protein facilitates chronic infection (57). Molecular chaperones like SecB, IbpA, and HtpG were downregulated in attached PAO1 Δfap cells (Fig. 7E). SecB exports proteins, and IbpA controls antiaging effects of a subpopulation by maintaining protein degradasome and folding homeostasis (58). HtpG is related to biofilm formation and, importantly, adhesion to surfaces (59).

DISCUSSION

We initiated this study to explore the significance of the conservation and evolution of the Fap system into an operon by *P. aeruginosa* (18, 19). To address this question, a

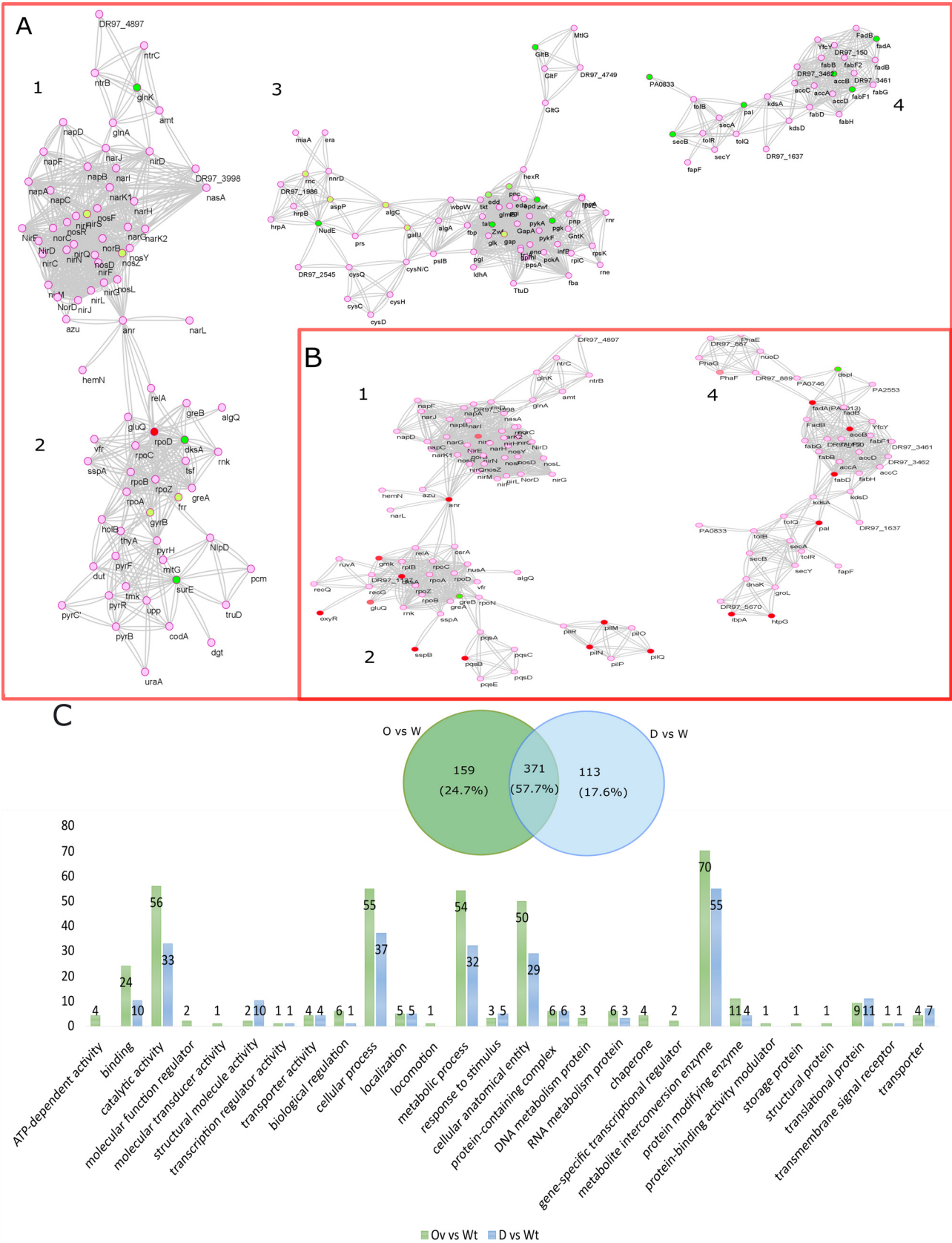


FIG 6 Fap influence protein interaction network and GO classification of differential proteomics. Comparative interactive networks in the presence and absence of Fap system denoting activation (green and yellow nodes based on decreasing values of log-fold change) and suppression (red and (Continued on next page)

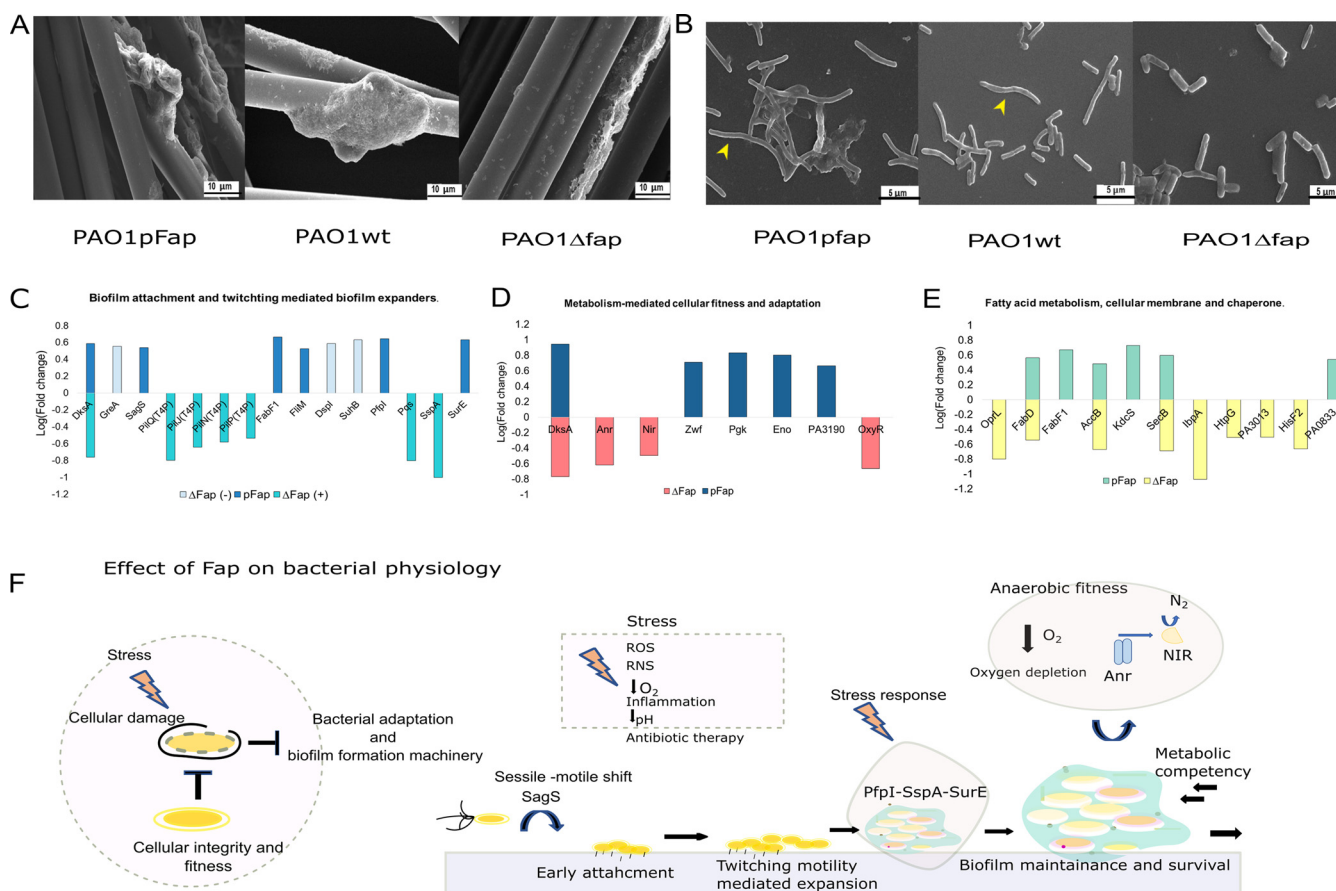


FIG 7 Fap-influenced bacterial phenotypical changes, differentially expressed proteins, and theoretical model demonstrating Fap-mediated adaptations. (A) SEM images of surface-attached biofilm of different Fap variants taken for surface-associated proteomics. (B) SEM images of SIP of different Fap variants taken for proteomics; yellow arrows indicate presence of elongated cellular morphology in PAO1 pFap and PAO1 wt groups, while rod-like morphology was observed in Δfap. (C) Proteomics comparison of biofilm attachment and twitching-mediated biofilm expanders, where log (fold change) of important proteins was related to each genetic variant. (D) Metabolism-mediated cellular fitness and adaptation proteins comparison between Fap variants. (E) Important differentially expressed proteins associated with cellular integrity, fatty acid synthesis, and chaperone. (F) Schematic model representing functionality of different protein hubs in biofilm formation and maintenance of biofilm, and also stress response under the influence of Fap expression. Δfap(−) represents protein expression that inversely affected biofilm formation, while Δfap(+) represents proteins that were positively correlated with biofilm. pFap(+) represents proteins positively affecting biofilm formation.

in vivo rat lung infection model and surface-associated proteomics were utilized. The *in vivo* study demonstrated essentiality of *P. aeruginosa* in generating pulmonary infection. Differential proteomics of *P. aeruginosa* PAO1 Fap variants indicated selective expression of pathoadaptive proteins that correlated with histopathological manifestations. Moreover, the surface-associated proteomics study delineated that Fap expression necessitates global proteome changes associated with mechano-sensing and physiological modulation, which reinforce *P. aeruginosa* biofilm sustainability. Reportedly, an exopolysaccharide-driven aggregated phenotype akin to biofilm is found in CF sputum and obstructs innate defenses (60). Marked to moderate bacterial aggregation was revealed by amyloid-producing strains in a pulmonary environment and the *in vitro* whole-blood system. At a molecular level, two critical regulators were responsible for the biofilm formation and continuum, as DksA and SagS were positively associated with Fap expression. DksA via ppGpp regulates the stringent stress

FIG 6 Legend (Continued)

salmon nodes based on decreasing values of log-fold change) in critical protein interactomes. (A) Interactome status in overexpressed system. 1, anaerobic pathway and nitrogen regulatory hub; 2, biofilm formation and maintenance hub; 3, glucose and pathoadaptation hub; 4, fatty acid, membrane proteins, and chaperone hub. (B) Interactome status in the absence of Fap. 1, anaerobic pathway and nitrogen regulatory hub; 2, biofilm formation, maintenance, and attachment hub; 4, dispersion, fatty acid, membrane proteins, and chaperone hub. (C) GO classification of proteins exclusive to O versus W and D versus W proteome. Bar graph demonstrates clustering of number of proteins to certain functional class in respective group (O versus W and D versus W is PAO1 pFap versus PAO1 wt and PAO1 Δfap versus PAO1 wt).

response and cellular persistence, while SagS, necessary for chronic infections, controls the phosphorylation cascade that generates continuous biofilm sustainability (30, 35, 61). The bacterial aggregates akin to *in vitro* biofilm downregulate virulence factors, which consequentially decrease host immunostimulation (62). The aggregative phenotype evokes the innate neutrophilic response, but the biofilm matrix shields from phagocytosis and host antimicrobials (62). Moreover, the size of aggregates impedes phagocytosis as demonstrated by *in vitro* HWB infection. Recruited neutrophils produce elevated neutrophil elastase, which further compromises bacterial clearance and causes airway destruction, as evident in histopathological observations (6, 63).

The neutrophilic activities deplete the limited oxygen supply in the pulmonary environment for *P. aeruginosa* (10, 64). This situation pushes the “obligate aerobe” to activate denitrification pathways and opt for an anaerobic lifestyle (10). The rod-like PAO1 Δfap phenotype, with significant downregulation of Anr and DksA, suggests a defect in anaerobic pathoadaptation. Furthermore, an interactive network showed that Anr, Nir, and Fap regulons were interconnected (data not shown). The absence of Fap suppressed the interactomes associated with biofilm formation, stress response, and cellular integrity in PAO1 Δfap and effaced matrix-mediated defense, leading to decreased pathogenesis. The DksA involvement in infection establishment and motility regulation explained why its downregulation in PAO1 Δfap affected initial attachment to lung surfaces (65). Higher Dsps and SuhB expression levels shifted PAO1 Δfap to planktonic lifestyle, making it susceptible to host immune response, bacterial clearance, and mild bacteremia in the HWB model. Furthermore, the suppressed chaperone activity was associated with the dysregulated protein homeostasis necessary for cellular fitness. Moreover, OxyR-mediated protection against bacterial clearance and neutrophil evasion was compromised due to its suppression in PAO1 Δfap (47).

Interestingly, the PAO1 pFap strain generated an end-stage (late-stage) emphysema CF pathology without underlying genetic disorder. Fap overexpression modulated bacterial physiology akin to CF isolates by upregulating pathoadaptive proteins (CF selected) that can derive nutrition, survive CF airway stress, and persist (53). Upregulation of glucose metabolism proteins Zwf, Eno, Pgi, PA3190, and OprB-glucose uptake suggested utilization of increased glucose in airway surface liquid (ASL), as found in CF-related diabetes (CFRD) (66). Proteins associated with cellular integrity, exopolysaccharide production (AlgC), and osmoprotection (OsmE and BetA) enabled survival and persistence in the mucus-ridden CF pathology (53). Furthermore, the increased levels of systemic IL-1 β in the pFap group suggested activated inflammasomes causing uncontrolled inflammation, compromised bacterial clearance, and development of chronic infection (67).

In conclusion, the Fap system is conserved in *P. aeruginosa* to provide cellular fitness for lung colonization, establishment of infection, and persistence. Presence of Fap had immunomodulatory consequences that produced hyperinflammation-mediated chronic infection. Moreover, Fap induces expression of “CF-selected” protein, signifying inextricably linkage with CF lung colonizers. Hence, the conservation, extracellular localization, and involvement of Fap in infection make this protein a target for interventions. Further study is warranted to understand host-pathogen interaction and immunological responses activated by the Fap system.

MATERIALS AND METHODS

In vitro studies. (i) Bacterial strains. *P. aeruginosa* PAO1 wt (wild-type strain) (68), PAO1 Δfap (Fap operon deleted in PAO1 wt) (69), and PAO1 pFap (Fap operon cloned in a pMMB190Tc vector transformed in PAO1 wt) (69) were grown on Luria-Bertani (LB) agar plates at 37°C. PAO1 pFap was created by transformation of PAO1 wt with the pFap plasmid as previously described (69) and plated on LB plates supplemented with 70 μ g/mL tetracycline, 40 μ g/mL Congo red, and 20 μ g/mL Coomassie brilliant blue G-250. Tetracycline effectively assisted in the selection of the pFap overexpression plasmid in PAO1 pFap colonies, which were further evaluated based on their binding of Congo red and Coomassie brilliant blue (70). Liquid cultures of PAO1 pFap were obtained by inoculating LB medium supplemented with 70 μ g/mL tetracycline with a single colony and incubating the culture overnight at 37°C with agitation. Static biofilm relative quantification was determined in a microtiter plate crystal violet (CV) assay for 16 h, and colorimetric quantification was performed at 600 nm (71).

(ii) In vitro whole-blood infection studies. Human whole blood (HWB) was collected from Blood Bank JNMC, Aligarh following all safety guideline provided by the blood bank. Heparinized blood (90% final blood concentration) was incubated with bacterial inoculum of 10⁷ CFU/mL in Gibco RPMI 1640 medium. The coculture was incubated for 16 h at 37°C augmented with 5% CO₂ (72). The peripheral blood smear stained

with Leishman stain was observed at $\times 40$ magnification by light microscopy. The hemolytic activity of bacteria was carried for 16 h, and hemolysis was determined at 534 nm as previously described (73).

In vivo studies. (i) Ethics statement. The animal experiments were approved by the Institutional Animal Ethical Committee and the Committee for the Purpose of Control and Supervision of Experiments on Animals (reference number 1979/GO/Re/S/17/CPCSEA/20).

(ii) Animals. Female Wistar rats purchased from AIIMS (New Delhi, India) were inoculated with *Pseudomonas* variants as described below. The animals were maintained under controlled temperature (26°C) with 12-h dark-light cycle.

(iii) Rat lung infection model. Rats weighing 200 to 250 g (10 to 11 weeks old) were tracheotomized for bacterial instillation under anesthesia (exposure of 5 mL ether in desiccator for 2 min augmented with intramuscular ketamine at 100 mg/kg) (74). A bacterial inoculum size of 200 μ L containing 10^7 CFU of PAO1 wt (group 1), PAO1 pFap (group 2), or PAO1 Δ fap (group 3) in phosphate-buffered saline (PBS) was used for instillation. PBS without bacteria was used as a negative control (group 4). The sutured incisions healed without complications. The rats were allowed to recover, and the infection progression was monitored after 3, 7, and 11 days. Three rats from each group were sacrificed at the aforementioned times, and the lungs were removed aseptically. Tissue homogenates of the lungs were serially diluted and 100- μ L samples plated on Mueller-Hinton agar plates to determine the bacterial load in CFU per gram of organ. The remaining lung tissues were fixed for histopathological analyses (75, 76).

(iv) Cytokine assays. The preinstillation and postinstillation sera were collected and stored at -20°C until analyzed. The following kits were used to assess the cytokines by enzyme-linked immunosorbent assay (ELISA), all obtained from Elabscience: IL-6 (catalog number E-EL-R0015), IFN- γ (catalog number E-EL-R0009), IL-1 β (catalog number E-EL-R0012), and RayBio TNF- α (catalog number ELR-TNFa-1).

(v) Histopathological sample preparation. Lung tissues were fixed in 10% neutral buffered saline and embedded in paraffin blocks. Tissue sections of 5 μ m were prepared as previously described (77). These sections were stained with hematoxylin and eosin and then mounted by using diphenylxylene (DPX). The slides were visualized at $\times 10$ and $\times 40$ magnification. Histopathological scoring of lung tissues was done by grades: marked (3+), moderate (2+), or mild (+), based on degree of pathological manifestation and amount of tissue affected (78).

(vi) SEM. The lung tissues were prepared for SEM as previously described (76). The sections were mounted on sample stubs and coated with gold-palladium. Samples were analyzed on three magnifications: $\times 200$, $\times 500$, and $\times 2,500$.

(vii) CLSM. For confocal laser scanning microscopy (CLSM), the tissue sections were cut at 8 μ m and subsequently deparaffinized by 100% xylene. The tissue sections were stained by Congo red and Thioflavin T as previously described (79, 80). A Fluoview FV1000 CLSM (Olympus, Tokyo, Japan) was used to analyze samples at the excitation wavelengths of 561 nm and 405 nm for Congo red and Thioflavin T, respectively. The emission wavelengths were set at 580 nm and 450 nm for Congo red and Thioflavin T, respectively.

Surface-associated proteomics study. (i) Bacterial strains and growth conditions. Colonies of PAO1 wt, PAO1 Δ fap, and PAO1 pFap grown on LB agar plates were used to inoculate colonization factor antigen (CFA) medium (70) and create overnight cultures. The medium of PAO1 pFap was supplemented with 70 μ g/mL tetracycline to maintain the plasmid. A 10% inoculum of each variant was seeded separately into 300 mL CFA containing 3 g glass wool (Merck Millipore catalog number 104086) that covered the base area of a 500-mL Erlenmeyer flask, as previously described (25). All the Fap variant cultures were induced with 0.8 mM isopropyl- β -D-thiogalactopyranoside (IPTG) for PAO1 pFap after 5 h, and all cultures were grown for 16 h, 18 h, and 22 h to obtain different biofilm states.

(ii) Scanning electron microscopy and confocal microscopy. The glass wool samples treated with 2% formaldehyde and 2.5% glutaraldehyde solution in PBS were incubated for 1 h at 4°C , followed by dehydration by an increasing ethanol gradient (20 to 100%). The samples were dried, sputter coated with gold-palladium, and then analyzed with SEM as previously described (81). The SEM images for biofilm and SIP groups were taken at $\times 1,000$ and $\times 5,000$, respectively. For confocal fluorescence microscopy, the glass wool samples were stained with propidium iodide and Syto9 and analyzed as previously described (82).

(iii) Sample preparation for proteomics. The samples were divided in two categories: (i) cells adhered to glass wool fiber (biofilm mass) and (ii) planktonic cells (for SIP). Prior to sample collection, biofilms at different time points were analyzed via SEM and CLSM. Due to viability issues, biofilm samples from 16 h were studied.

SIP biomass was pelleted by centrifugation at $3,381 \times g$ for 10 min and washed with PBS prior to storage at -80°C .

(iv) Biofilm mass extraction. The glass wool was washed three times with 50 mL of a 0.85% NaCl solution to remove weakly attached cells. After this initial washing, 50 mL of 0.85% NaCl was added along with 30 g of glass beads (mean diameter, 4 mm). The flasks were agitated for 20 min to detach adherent cells, and liquid was collected. An additional 50 mL of 0.85% NaCl was added to the glass wool and agitation was repeated to detach the remaining adhered cells. The combined cell suspension was pelleted at $3,381 \times g$ for 10 min, after which the pellet was washed once in PBS and stored at -80°C as previously described (83).

(v) Protein extraction. For protein extraction, the pellet was dissolved in lysis buffer (50 mM Tris-HCl [pH 7.2], 300 mM NaCl, 2 mM dithiothreitol, and 1 mM phenylmethylsulfonyl fluoride) followed by ultrasonication (QSonica Q700; 30 W, pulse on for 20 s and pulse off for 5 s for 15 min at 4°C). The lysate was subjected to centrifugation for $(4,200 \times g)$ for 10 min to remove cellular debris. The supernatant was subjected to centrifugation $(13,523 \times g)$ for 30 min to obtain the soluble and insoluble fractions. The insoluble pellet was washed with PBS, redissolved, and boiled in lysis buffer containing 2% (vol/vol) SDS for 20 min. The SDS-PAGE loading buffer ($2\times$) was added to the soluble and insoluble fractions. The quantitated protein samples were loaded in equal amounts on a 12% SDS-PAGE gel. The SDS-PAGE was carried out at a constant voltage (100 V, 1 h). The SDS-PAGE was stained with Coomassie R250, and the

sample lanes were cut and further excised in 5 pieces. In-gel trypsin digestion was performed as previously described (84), and samples were stored at -20°C until analyzed by mass spectrometer.

Mass spectrometry. (i) Identification. (a) *Shotgun analysis for protein identification and its acquisition parameters.* An information-dependent acquisition (IDA) process was utilized, in which the MS1 scan determined the mass-to-charge ratio (m/z) and the abundance of ions that entered the mass spectrometer, followed by tandem mass spectrometry (MS/MS) fragmentation from a subset of detected peaks (85). The setup was as follows: one full MS scan (m/z 350 to 1,250) with accumulation time of 250 ms, followed by 35 data-dependent MS/MS spectra (m/z 100 to 1,800) with an accumulation time of 50 ms in each cycle and a total cycle time of ~ 2.5 to 3.0 s.

Tryptic peptides suspended in solvent A (2% [vol/vol] acetonitrile, 0.1% [vol/vol] formic acid in water) were analyzed with a Sciex 5600+ Triple-time of flight (TOF) mass spectrometer coupled with a BEH column (C_{18} , $1.7\ \mu\text{m}$) in an Exigent ultraperformance liquid chromatography (UPLC) system. The peptides were separated using a 60-min linear acetonitrile gradient starting from 5 to 50% solvent B (98:2% [vol/vol] acetonitrile-water, 0.1% [vol/vol] formic acid) at a flow rate of $300\ \mu\text{L}/\text{min}$ with column temperature of 40°C . Data of each fraction were acquired in electrospray ionization positive mode. A maximum of 35 precursor ions with charge states of 2 to 5 that surpassed 100 cps per cycle were selected for fragmentation, and each MS/MS spectrum was accumulated in high-sensitivity mode with dynamic exclusion to 8 to 10 s, as previously described with slight modifications (86). The LC-MS instrument was calibrated prior to each sample set acquisition with *Escherichia coli* β -galactosidase (BGAL_ECOLI-[P00722]) tryptic digest to maintain the mass within an accuracy of ± 2 ppm mass range for MS and MS/MS.

(b) *Shotgun data analysis.* IDA data were processed with Protein Pilot software v. 5.03 (Sciex, Foster City, CA, USA), where a 1% false-discovery rate (FDR) with statistical significance was set for peptides. In brief, the *Pseudomonas* protein database with 5,586 protein entries (www.pseudomonas.com assembly accession number GCF_000006765.1) was used for protein identification.

(i) Quantification. (a) *Data-independent acquisition SWATH and its acquisition parameters.* SWATH is a data-independent acquisition (DIA) method was used for quantification which depends on a previously generated peptide spectral library by shotgun proteomics (87).

First, protein digests (5 to $10\ \mu\text{g}$) of all samples were analyzed using the SWATH method in the first experiment. Second, we spiked 1 pmol of tryptic peptides derived from *E. coli* β -galactosidase (β -Gal) into $5\ \mu\text{g}$ of cell lysate digest. All samples were spiked with the equal concentration of β -Gal protein. The β -Gal-containing samples were analyzed by SWATH as well.

Equal quantities of proteins samples digested by trypsin were subjected to DIA (SWATH). The peptides were analyzed using a Sciex Triple TOF 5600 mass spectrometer (SCIEX, USA) equipped with an Exion UPLC connected to an Acquity Premier Peptide BEH C_{18} column ($130\ \text{\AA}$, $1.7\ \mu\text{m}$, $2.1 \times 150\ \text{mm}$). SWATH was performed for the individual samples to generate high-quality spectral ion libraries by operating the mass spectrometer with specific parameters as previously described, with slight modification (88). Technical triplicates of SWATH were carried out for each sample in order to perform a t test.

(b) *SWATH data analysis.* The identified peptides and their corresponding fragment ions were prepared for subsequent spectral library match in the SWATH peak extraction. The peak extraction and spectral alignment were performed using Peakview software (version 2.2; SCIEX, USA). This information was extracted with the SWATH acquisition MicroApp (SWATH 2.0) in Peakview 2.2 software, during library extraction along with other information that was used for peptide and fragment selection within the MicroApp (SWATH 2.0), five transition ions per peptide (b or y ions) and two peptides per protein to be used, and all shared and modified peptides were excluded from the extraction. Further, retention time was realigned according to the manually selected 5 peptides that constantly had high signal intensities and were distributed along the whole-time chromatographic axis. All the quantified peptides were required to have FDRs of $< 1\%$. After normalization, principal-component analysis was performed to check the possible correlated variables within the group. The data were further subjected to analysis with MarkerView software (version 1.3.1; SCIEX, USA) for statistical data interpretation. In MarkerView, the results were shown as three output files containing the areas under the curves for the ions, the summed intensity of peptides for protein, and the summed intensity of ions for the peptide. We plotted a volcano curve to determine the statistically significant fold change versus P value for each comparative group. Proteins with a significant log fold change of 0.50 (increase or decrease), with a P value of ≤ 0.05 were considered up- or downregulated proteins, respectively.

Bioinformatic analysis of proteomic data. The differential abundant proteins were clustered by the following Genetic Ontology classifications: MF, molecular function, i.e., gene products that produce molecular-like activities; BP, biological process, i.e., gene products associated with large biological programs performed by multiple molecular activities; CC, cellular component, i.e., class of gene products associated with anatomical structures of cells; PC, protein classes, i.e., protein families grouping based on their broad functional classes (89). The interaction networks were exported from the STRING 2.0 database to Cytoscape 3.8 (90).

Statistical analysis. GraphPad prism 8.0 was used to represent all data in the form of averages \pm standard deviations (SD). One-way analysis of variance (ANOVA) was used to compare the multiple means of groups with respect to PAO1 wt. P values of < 0.05 were considered statistically significant. In biofilm studies, triplicates were considered, while in cytokine assays duplicates were considered.

Data availability. The proteomics data are available at the ProteomeXchange Consortium (<http://www.proteomexchange.org>) through its partner, the PRIDE repository, with project ID PXD033853.

ACKNOWLEDGMENTS

A.U.K. acknowledges Department of Biotechnology grant BT/PR40148/BTIS/137/20/2021 for support of this study. The University Sophisticated Instrumentation Facilities of

Aligarh Muslim University are acknowledged. The CSIR (SRF) fellowship of A.Z.B. is also acknowledged. We declare no conflicts of interest.

REFERENCES

- Emerson J, Rosenfeld M, McNamara S, Ramsey B, Gibson RL. 2002. *Pseudomonas aeruginosa* and other predictors of mortality and morbidity in young children with cystic fibrosis. *Pediatr Pulmonol* 34:91–100. <https://doi.org/10.1002/ppul.10127>.
- Merakou C, Schaefer MM, Priebe GP. 2018. Progress toward the elusive *Pseudomonas aeruginosa* vaccine. *Surg Infect (Larchmt)* 19:757–768. <https://doi.org/10.1089/sur.2018.233>.
- Scheetz MH, Hoffman M, Bolon MK, Schultert G, Estrellado W, Baraboutis IG, Sriram P, Dinh M, Owens LK, Hauser AR. 2009. Morbidity associated with *Pseudomonas aeruginosa* bloodstream infections. *Diagn Microbiol Infect Dis* 64:311–319. <https://doi.org/10.1016/j.diagmicrobio.2009.02.006>.
- Francolini I, Donelli G. 2010. Prevention and control of biofilm-based medical device-related infections. *FEMS Immunol Med Microbiol* 59:227–238. <https://doi.org/10.1111/j.1574-695X.2010.00665.x>.
- Mulcahy LR, Isabella VM, Lewis K. 2014. *Pseudomonas aeruginosa* biofilms in disease. *Microb Ecol* 68:1–12. <https://doi.org/10.1007/s00248-013-0297-x>.
- Montgomery ST, Mall MA, Kicic A, Stick SM. 2017. Hypoxia and sterile inflammation in cystic fibrosis airways: mechanisms and potential therapies. *Eur Respir J* 49:1600903. <https://doi.org/10.1183/13993003.00903-2016>.
- Burns JL, Gibson RL, McNamara S, Yim D, Emerson J, Rosenfeld M, Hiatt P, McCoy K, Castile R, Smith AL, Ramsey BW. 2001. Longitudinal assessment of *Pseudomonas aeruginosa* in young children with cystic fibrosis. *J Infect Dis* 183:444–452. <https://doi.org/10.1086/318075>.
- Mayer-Hamblett N, Kloster M, Rosenfeld M, Gibson RL, Retsch-Bogart GZ, Emerson J, Thompson V, Ramsey BW. 2015. Impact of sustained eradication of new *Pseudomonas aeruginosa* infection on long-term outcomes in cystic fibrosis. *Clin Infect Dis* 61:707–715. <https://doi.org/10.1093/cid/civ377>.
- Malhotra S, Hayes D, Jr, Wozniak DJ. 2019. Cystic fibrosis and *Pseudomonas aeruginosa*: the host-microbe interface. *Clin Microbiol Rev* 32:e00138-18. <https://doi.org/10.1128/CMR.00138-18>.
- Lin CK, Kazmierczak BI. 2017. Inflammation: a double-edged sword in the response to *Pseudomonas aeruginosa* infection. *J Innate Immun* 9:250–261. <https://doi.org/10.1159/000455857>.
- Boisvert A-A, Cheng MP, Sheppard DC, Nguyen D. 2016. Microbial biofilms in pulmonary and critical care diseases. *Ann Am Thorac Soc* 13:1615–1623. <https://doi.org/10.1513/AnnalsATS.201603-194FR>.
- Horcajada JP, Montero M, Oliver A, Sorli L, Luque S, Gómez-Zorrilla S, Benito N, Grau S. 2019. Epidemiology and treatment of multidrug-resistant and extensively drug-resistant *Pseudomonas aeruginosa* infections. *Clin Microbiol Rev* 32:e00031-19. <https://doi.org/10.1128/CMR.00031-19>.
- Wei Q, Ma LZ. 2013. Biofilm matrix and its regulation in *Pseudomonas aeruginosa*. *Int J Mol Sci* 14:20983–21005. <https://doi.org/10.3390/ijms141020983>.
- Borlee BR, Goldman AD, Murakami K, Samudrala R, Wozniak DJ, Parsek MR. 2010. *Pseudomonas aeruginosa* uses a cyclic-di-GMP-regulated adhesin to reinforce the biofilm extracellular matrix. *Mol Microbiol* 75:827–842. <https://doi.org/10.1111/j.1365-2958.2009.06991.x>.
- Diggle SP, Stacey RE, Dodd C, Cámara M, Williams P, Winzer K. 2006. The galactophilic lectin, LecA, contributes to biofilm development in *Pseudomonas aeruginosa*. *Environ Microbiol* 8:1095–1104. <https://doi.org/10.1111/j.1462-2920.2006.001001.x>.
- Zeng G, Vad BS, Dueholm MS, Christiansen G, Nilsson M, Tolker-Nielsen T, Nielsen PH, Meyer RL, Otzen DE. 2015. Functional bacterial amyloid increases *Pseudomonas* biofilm hydrophobicity and stiffness. *Front Microbiol* 6:1099. <https://doi.org/10.3389/fmicb.2015.01099>.
- Seviour T, Hansen SH, Yang L, Yau YH, Wang VB, Stenvang MR, Christiansen G, Marsili E, Givskov M, Chen Y, Otzen DE, Nielsen PH, Geifman-Shochat S, Kjelleberg S, Dueholm MS. 2015. Functional amyloids keep quorum-sensing molecules in check. *J Biol Chem* 290:6457–6469. <https://doi.org/10.1074/jbc.M114.613810>.
- Rouse SL, Matthews SJ, Dueholm MS. 2018. Ecology and biogenesis of functional amyloids in *Pseudomonas*. *J Mol Biol* 430:3685–3695. <https://doi.org/10.1016/j.jmb.2018.05.004>.
- Beg AZ, Farhat N, Khan AU. 2021. Designing multi-epitope vaccine candidates against functional amyloids in *Pseudomonas aeruginosa* through immunoinformatic and structural bioinformatics approach. *Infect Genet Evol* 93:104982. <https://doi.org/10.1016/j.meegid.2021.104982>.
- Dueholm MS, Otzen D, Nielsen PH. 2013. Evolutionary insight into the functional amyloids of the pseudomonads. *PLoS One* 8:e76630. <https://doi.org/10.1371/journal.pone.0076630>.
- Kim J-Y, Sahu S, Yau Y-H, Wang X, Shochat SG, Nielsen PH, Dueholm MS, Otzen DE, Lee J, Delos Santos MMS, Yam JKH, Kang N-Y, Park S-J, Kwon H, Seviour T, Yang L, Givskov M, Chang Y-T. 2016. Detection of pathogenic biofilms with bacterial amyloid targeting fluorescent probe, CDY11. *J Am Chem Soc* 138:402–407. <https://doi.org/10.1021/jacs.5b11357>.
- Tükel Ç, Nishimori JH, Wilson RP, Winter MG, Keestra AM, Van Putten JPM, Bäuml AJ. 2010. Toll-like receptors 1 and 2 cooperatively mediate immune responses to curli, a common amyloid from enterobacterial biofilms. *Cell Microbiol* 12:1495–1505. <https://doi.org/10.1111/j.1462-5822.2010.01485.x>.
- Chen SG, Stribinskis V, Rane MJ, Demuth DR, Gozal E, Roberts AM, Jagadapillai R, Liu R, Choe K, Shivakumar B, Son F, Jin S, Kerber R, Adame A, Masliah E, Friedland RP. 2016. Exposure to the functional bacterial amyloid protein curli enhances alpha-synuclein aggregation in aged Fischer 344 rats and *Caenorhabditis elegans*. *Sci Rep* 6:34477. <https://doi.org/10.1038/srep34477>.
- Lin MT, Balczon R, Pittet J-F, Wagener BM, Moser SA, Morrow KA, Voth S, Francis CM, Leavesley S, Bell J, Alvarez DF, Stevens T. 2018. Nosocomial pneumonia elicits an endothelial proteinopathy: evidence for a source of neurotoxic amyloids in critically ill patients. *Am J Respir Crit Care Med* 198:1575–1578. <https://doi.org/10.1164/rccm.201801-0060LE>.
- Steyn B, Oosthuizen MC, MacDonald R, Theron J, Brözel VS. 2001. The use of glass wool as an attachment surface for studying phenotypic changes in *Pseudomonas aeruginosa* biofilms by two-dimensional gel electrophoresis. *Proteomics* 1:871–879. [https://doi.org/10.1002/1615-9861\(200107\)1:7<871::AID-PROT871>3.0.CO;2-2](https://doi.org/10.1002/1615-9861(200107)1:7<871::AID-PROT871>3.0.CO;2-2).
- Hare NJ, Cordwell SJ. 2010. Proteomics of bacterial pathogens: *Pseudomonas aeruginosa* infections in cystic fibrosis, a case study. *Proteomics Clin Appl* 4:228–248. <https://doi.org/10.1002/prca.200900144>.
- Mets OM, Roothaan SM, Bronsveld I, Luijk B, van de Graaf EA, Vink A, de Jong PA. 2015. Emphysema is common in lungs of cystic fibrosis lung transplantation patients: a histopathological and computed tomography study. *PLoS One* 10:e0128062. <https://doi.org/10.1371/journal.pone.0128062>.
- Savaşan S, Bhambhani K, Abdulhamid I, Ravindranath Y. 1997. Cystic fibrosis and anaemia in infancy. *Lancet* 350:295. [https://doi.org/10.1016/S0140-6736\(05\)62265-9](https://doi.org/10.1016/S0140-6736(05)62265-9).
- Van Heeckeren AM, Tscheikuna J, Walenga RW, Konstan MW, Davis PB, Erokku B, Haxhiu MA, Ferkol TW. 2000. Effect of *Pseudomonas* infection on weight loss, lung mechanics, and cytokines in mice. *Am J Respir Crit Care Med* 161:271–279. <https://doi.org/10.1164/ajrccm.161.1.9903019>.
- Min KB, Yoon SS. 2020. Transcriptome analysis reveals that the RNA polymerase-binding protein DksA1 has pleiotropic functions in *Pseudomonas aeruginosa*. *J Biol Chem* 295:3851–3864. <https://doi.org/10.1074/jbc.RA119.011692>.
- Nolan LM, Whitchurch CB, Barquist L, Katrib M, Boinett CJ, Mayho M, Goulding D, Charles IG, Filloux A, Parkhill J. 2018. A global genomic approach uncovers novel components for twitching motility-mediated biofilm expansion in *Pseudomonas aeruginosa*. *Microb Genom* 4:e000229. <https://doi.org/10.1099/mgen.0.000229>.
- O'Toole GA, Kolter R. 1998. Flagellar and twitching motility are necessary for *Pseudomonas aeruginosa* biofilm development. *Mol Microbiol* 30:295–304. <https://doi.org/10.1046/j.1365-2958.1998.01062.x>.
- Rodríguez-Rojas A, Blázquez J. 2009. The *Pseudomonas aeruginosa* pfl gene plays an antimitigator role and provides general stress protection. *J Bacteriol* 191:844–850. <https://doi.org/10.1128/JB.01081-08>.
- Castaneda RJ, Freeman SA, Riggan M, Song-Zhao GX. 2007. Identification of a novel caspase-3-like protease, Clp, in *Pseudomonas aeruginosa* biofilms and its modulation of rapid cell death. *J Exp Microbiol Immunol* 11:23–29.
- Park S, Sauer K. 2021. SagS and its unorthodox contributions to *Pseudomonas aeruginosa* biofilm development. *Biofilm* 3:100059. <https://doi.org/10.1016/j.biofilm.2021.100059>.
- Diggle SP, Winzer K, Chhabra SR, Worrall KE, Cámara M, Williams P. 2003. The *Pseudomonas aeruginosa* quinolone signal molecule overcomes the cell density-dependency of the quorum sensing hierarchy, regulates rhl-dependent genes at the onset of stationary phase and can be produced in the absence of LasR. *Mol Microbiol* 50:29–43. <https://doi.org/10.1046/j.1365-2958.2003.03672.x>.

37. Liu L, Li T, Cheng X-J, Peng C-T, Li C-C, He L-H, Ju S-M, Wang N-Y, Ye T-H, Lian M, Xiao Q-J, Song Y-J, Zhu Y-B, Yu L-T, Wang Z-L, Bao R. 2018. Structural and functional studies on *Pseudomonas aeruginosa* DspI: implications for its role in DSF biosynthesis. *Sci Rep* 8:12632. <https://doi.org/10.1038/s41598-018-30920-w>.
38. Li K, Yang G, Debru AB, Li P, Zong L, Li P, Xu T, Wu W, Jin S, Bao Q. 2017. SuhB regulates the motile-sessile switch in *Pseudomonas aeruginosa* through the Gac/Rsm pathway and c-di-GMP signaling. *Front Microbiol* 8: 1045. <https://doi.org/10.3389/fmicb.2017.01045>.
39. Ozdemir OO, Soyer F. 2020. *Pseudomonas aeruginosa* presents multiple vital changes in its proteome in the presence of 3-hydroxyphenylacetic acid, a promising antimicrobial agent. *ACS Omega* 5:19938–19951. <https://doi.org/10.1021/acsomega.0c00703>.
40. Drabinska J, Ziecina M, Modzelan M, Jagura-Burdzy G, Kraszevska E. 2020. Individual Nudix hydrolases affect diverse features of *Pseudomonas aeruginosa*. *Microbiologyopen* 9:e1052. <https://doi.org/10.1002/mbo3.1052>.
41. Paul D, Dineshkumar N, Nair S. 2006. Proteomics of a plant growth-promoting rhizobacterium, *Pseudomonas fluorescens* MSP-393, subjected to salt shock. *World J Microbiol Biotechnol* 22:369–374. <https://doi.org/10.1007/s11274-005-9043-y>.
42. Yoon MY, Lee K-M, Park Y, Yoon SS. 2011. Contribution of cell elongation to the biofilm formation of *Pseudomonas aeruginosa* during anaerobic respiration. *PLoS One* 6:e16105. <https://doi.org/10.1371/journal.pone.0016105>.
43. Silo-Suh L, Suh S-J, Phibbs PV, Ohman DE. 2005. Adaptations of *Pseudomonas aeruginosa* to the cystic fibrosis lung environment can include deregulation of zwf, encoding glucose-6-phosphate dehydrogenase. *J Bacteriol* 187:7561–7568. <https://doi.org/10.1128/JB.187.22.7561-7568.2005>.
44. Weng Y, Chen F, Liu Y, Zhao Q, Chen R, Pan X, Liu C, Cheng Z, Jin S, Jin Y, Wu W. 2016. *Pseudomonas aeruginosa* enolase influences bacterial tolerance to oxidative stresses and virulence. *Front Microbiol* 7:1999. <https://doi.org/10.3389/fmicb.2016.01999>.
45. Deng X, Liang H, Ulanovskaya OA, Ji Q, Zhou T, Sun F, Lu Z, Hutchison AL, Lan L, Wu M, Cravatt BF, He C. 2014. Steady-state hydrogen peroxide induces glycolysis in *Staphylococcus aureus* and *Pseudomonas aeruginosa*. *J Bacteriol* 196:2499–2513. <https://doi.org/10.1128/JB.01538-14>.
46. Chevalier S, Bouffartigues E, Bodilis J, Maillot O, Lesouhaitier O, Feuilloley MGJ, Orange N, Dufour A, Cornelis P. 2017. Structure, function and regulation of *Pseudomonas aeruginosa* porins. *FEMS Microbiol Rev* 41:698–722. <https://doi.org/10.1093/femsre/fux020>.
47. Lau GW, Britigan BE, Hassett DJ. 2005. *Pseudomonas aeruginosa* OxyR is required for full virulence in rodent and insect models of infection and for resistance to human neutrophils. *Infect Immun* 73:2550–2553. <https://doi.org/10.1128/IAI.73.4.2550-2553.2005>.
48. Llamas MA, Rodríguez-Herva JJ, Hancock REW, Bitter W, Tommassen J, Ramos JL. 2003. Role of *Pseudomonas putida* tol-oprL gene products in uptake of solutes through the cytoplasmic membrane. *J Bacteriol* 185: 4707–4716. <https://doi.org/10.1128/JB.185.16.4707-4716.2003>.
49. Tahrioui A, Ortiz S, Azuama OC, Bouffartigues E, Benalia N, Tortuel D, Maillot O, Chemat S, Kritsanida M, Feuilloley M, Orange N, Michel S, Lesouhaitier O, Cornelis P, Grougnet R, Bouffartigues S, Chevalier S. 2020. Membrane-interactive compounds from *Pistacia lentiscus* L. thwart *Pseudomonas aeruginosa* virulence. *Front Microbiol* 11:1068. <https://doi.org/10.3389/fmicb.2020.01068>.
50. Kutchma AJ, Hoang TT, Schweizer HP. 1999. Characterization of a *Pseudomonas aeruginosa* fatty acid biosynthetic gene cluster: purification of acyl carrier protein (ACP) and malonyl-coenzyme A:ACP transacylase (FabD). *J Bacteriol* 181:5498–5504. <https://doi.org/10.1128/JB.181.17.5498-5504.1999>.
51. Sun Z, Kang Y, Norris MH, Troyer RM, Son MS, Schweizer HP, Dow SW, Hoang TT. 2014. Blocking phosphatidylcholine utilization in *Pseudomonas aeruginosa*, via mutagenesis of fatty acid, glycerol and choline degradation pathways, confirms the importance of this nutrient source in vivo. *PLoS One* 9:e103778. <https://doi.org/10.1371/journal.pone.0103778>.
52. King JD, Kocincová D, Westman EL, Lam JS. 2009. Lipopolysaccharide biosynthesis in *Pseudomonas aeruginosa*. *Innate Immun* 15:261–312. <https://doi.org/10.1177/1753425909106436>.
53. Dettman JR, Kassen R. 2021. Evolutionary genomics of niche-specific adaptation to the cystic fibrosis lung in *Pseudomonas aeruginosa*. *Mol Biol Evol* 38:663–675. <https://doi.org/10.1093/molbev/msaa226>.
54. Dong H, Ma J, Chen Q, Chen B, Liang L, Liao Y, Song Y, Wang H, Cronan JE. 2021. A cryptic long-chain 3-ketoacyl-ACP synthase in the *Pseudomonas putida* F1 unsaturated fatty acid synthesis pathway. *J Biol Chem* 297: 100920. <https://doi.org/10.1016/j.jbc.2021.100920>.
55. Fabian BK, Foster C, Asher AJ, Elbourne LDH, Cain AK, Hassan KA, Tetu SG, Paulsen IT. 2020. Elucidating essential genes in plant-associated *Pseudomonas* protegens Pf-5 using transposon insertion sequencing. *J Bacteriol* 203:e00432-20. <https://doi.org/10.1128/JB.00432-20>.
56. Shu L, Chen S, Chen X, Lin S, Du X, Deng K, Wei J, Cao Y, Yan J, Shen Z. 2020. The *Pseudomonas aeruginosa* secreted protein PA3611 promotes bronchial epithelial cells epithelial-mesenchymal transition via integrin α v β 6-mediated TGF- β 1-induced p38/NF- κ B pathway activation. *Front Microbiol* 12:763749.
57. Yang F, Gu J, Zou J, Lei L, Jing H, Zhang J, Zeng H, Zou Q, Lv F, Zhang J. 2018. PA0833 is an OmpA C-like protein that confers protection against *Pseudomonas aeruginosa* infection. *Front Microbiol* 9:1062. <https://doi.org/10.3389/fmicb.2018.01062>.
58. Williamson KS, Richards LA, Perez-Osorio AC, Pitts B, McInerney K, Stewart PS, Franklin MJ. 2012. Heterogeneity in *Pseudomonas aeruginosa* biofilms includes expression of ribosome hibernation factors in the antibiotic-tolerant subpopulation and hypoxia-induced stress response in the metabolically active population. *J Bacteriol* 194:2062–2073. <https://doi.org/10.1128/JB.00022-12>.
59. Grudniak AM, Klecha B, Wolska KI. 2018. Effects of null mutation of the heat-shock gene *hspG* on the production of virulence factors by *Pseudomonas aeruginosa*. *Future Microbiol* 13:69–80. <https://doi.org/10.2217/fmb-2017-0111>.
60. Jennings LK, Dreifus JE, Reichardt C, Storek KM, Secor PR, Wozniak DJ, Hisert KB, Parsek MR. 2021. *Pseudomonas aeruginosa* aggregates in cystic fibrosis sputum produce exopolysaccharides that likely impede current therapies. *Cell Rep* 34:108782. <https://doi.org/10.1016/j.celrep.2021.108782>.
61. Moradali MF, Ghods S, Rehm BHA. 2017. *Pseudomonas aeruginosa* lifestyle: a paradigm for adaptation, survival, and persistence. *Front Cell Infect Microbiol* 7:39.
62. Faure E, Kwong K, Nguyen D. 2018. *Pseudomonas aeruginosa* in chronic lung infections: how to adapt within the host? *Front Immunol* 9:2416. <https://doi.org/10.3389/fimmu.2018.02416>.
63. Cabrini G, Rimessi A, Borgatti M, Lampronti I, Finotti A, Pinton P, Gambari R. 2020. Role of cystic fibrosis bronchial epithelium in neutrophil chemotaxis. *Front Immunol* 11:1438. <https://doi.org/10.3389/fimmu.2020.01438>.
64. Kragh KN, Alhede M, Jensen PØ, Moser C, Scheike T, Jacobsen CS, Seier Poulsen S, Eickhardt-Sørensen SR, Trøstrup H, Christoffersen L, Hougen H-P, Rickelt LF, Kühl M, Højby N, Bjarnsholt T. 2014. Polymorphonuclear leukocytes restrict growth of *Pseudomonas aeruginosa* in the lungs of cystic fibrosis patients. *Infect Immun* 82:4477–4486. <https://doi.org/10.1128/IAI.01969-14>.
65. Min KB, Hwang W, Lee K-M, Kim JB, Yoon SS. 2021. Chemical inhibitors of the conserved bacterial transcriptional regulator DksA1 suppressed quorum sensing-mediated virulence of *Pseudomonas aeruginosa*. *J Biol Chem* 296:100576. <https://doi.org/10.1016/j.jbc.2021.100576>.
66. Garnett JP, Gray MA, Tarran R, Brodrie M, Ward C, Baker EH, Baines DL. 2013. Elevated paracellular glucose flux across cystic fibrosis airway epithelial monolayers is an important factor for *Pseudomonas aeruginosa* growth. *PLoS One* 8:e76283. <https://doi.org/10.1371/journal.pone.0076283>.
67. Tang A, Sharma A, Jen R, Hirschfeld AF, Chilvers MA, Lavoie PM, Turvey SE. 2012. Inflammation-mediated IL-1 β production in humans with cystic fibrosis. *PLoS One* 7:e37689. <https://doi.org/10.1371/journal.pone.0037689>.
68. Jacobs MA, Alwood A, Thaipisuttikul I, Spencer D, Haugen E, Ernst S, Will O, Kaul R, Raymond C, Levy R, Chun-Rong L, Guenther D, Bovee D, Olson MV, Manoil C. 2003. Comprehensive transposon mutant library of *Pseudomonas aeruginosa*. *Proc Natl Acad Sci U S A* 100:14339–14344. <https://doi.org/10.1073/pnas.2036282100>.
69. Dueholm MS, Søndergaard MT, Nilsson M, Christiansen G, Stensballe A, Overgaard MT, Givskov M, Tolker-Nielsen T, Otzen DE, Nielsen PH. 2013. Expression of Fap amyloids in *Pseudomonas aeruginosa*, *P. fluorescens*, and *P. putida* results in aggregation and increased biofilm formation. *Microbiologyopen* 2:365–382. <https://doi.org/10.1002/mbo3.81>.
70. Herbst F-A, Søndergaard MT, Kjeldal H, Stensballe A, Nielsen PH, Dueholm MS. 2015. Major proteomic changes associated with amyloid-induced biofilm formation in *Pseudomonas aeruginosa* PAO1. *J Proteome Res* 14:72–81. <https://doi.org/10.1021/pr500938x>.
71. O'Toole GA. 2011. Microtiter dish biofilm formation assay. *J Vis Exp* 47:2437. <https://doi.org/10.3791/2437>.
72. Pont S, Fraikin N, Caspar Y, Van Melder L, Attrée I, Cretin F. 2020. Bacterial behavior in human blood reveals complement evaders with some persister-like features. *PLoS Pathog* 16:e1008893. <https://doi.org/10.1371/journal.ppat.1008893>.
73. Lee J-H, Kim Y-G, Cho MH, Lee J. 2014. ZnO nanoparticles inhibit *Pseudomonas aeruginosa* biofilm formation and virulence factor production. *Microbiol Res* 169:888–896. <https://doi.org/10.1016/j.micres.2014.05.005>.
74. de Magalhães RF, Samary CS, Santos RS, de Oliveira MV, Rocha NN, Santos CL, Kitoko J, Silva CAM, Hildebrandt CL, Gonçalves-de-Albuquerque CF, Silva AR, Faria-Neto HC, Martins V, Capelozzi VL, Huhle R, Morales MM,

- Olsen P, Pelosi P, de Abreu MG, Rocco PRM, Silva PL. 2016. Variable ventilation improves pulmonary function and reduces lung damage without increasing bacterial translocation in a rat model of experimental pneumonia. *Respir Res* 17:158. <https://doi.org/10.1186/s12931-016-0476-7>.
75. Torres BGS, Helfer VE, Bernardes PM, Macedo AJ, Nielsen EI, Friberg LE, Dalla Costa T. 2017. Population pharmacokinetic modeling as a tool to characterize the decrease in ciprofloxacin free interstitial levels caused by *Pseudomonas aeruginosa* biofilm lung infection in Wistar rats. *Antimicrob Agents Chemother* 61:e02553-16. <https://doi.org/10.1128/AAC.02553-16>.
 76. Kundu S, Sengupta S, Chatterjee S, Mitra S, Bhattacharyya A. 2009. Cadmium induces lung inflammation independent of lung cell proliferation: a molecular approach. *J Inflamm* 6:19. <https://doi.org/10.1186/1476-9255-6-19>.
 77. Sawaguchi A, Kamimura T, Yamashita A, Takahashi N, Ichikawa K, Aoyama F, Asada Y. 2018. Informative three-dimensional survey of cell/tissue architectures in thick paraffin sections by simple low-vacuum scanning electron microscopy. *Sci Rep* 8:7479. <https://doi.org/10.1038/s41598-018-25840-8>.
 78. Gibson-Corley KN, Olivier AK, Meyerholz DK. 2013. Principles for valid histopathologic scoring in research. *Vet Pathol* 50:1007–1015. <https://doi.org/10.1177/0300985813485099>.
 79. Picken MM, Herrera GA. 2015. Thioflavin T stain: an easier and more sensitive method for amyloid detection, p 225–227. *In* Picken MM, Herrera GA, Dogan A (ed), *Amyloid and related disorders*, 2nd ed. Springer, Cham, Switzerland.
 80. Garcia-Sherman MC, Lundberg T, Sobonya RE, Lipke PN, Klotz SA. 2015. A unique biofilm in human deep mycoses: fungal amyloid is bound by host serum amyloid P component. *NPJ Biofilms Microbiomes* 1:15009. <https://doi.org/10.1038/npjbiofilms.2015.9>.
 81. Dassanayake RP, Falkenberg SM, Stasko JA, Shircliff AL, Lippolis JD, Briggs RE. 2020. Identification of a reliable fixative solution to preserve the complex architecture of bacterial biofilms for scanning electron microscopy evaluation. *PLoS One* 15:e0233973. <https://doi.org/10.1371/journal.pone.0233973>.
 82. Vassena C, Fenu S, Giuliani F, Fantetti L, Roncucci G, Simonutti G, Romanò CL, De Francesco R, Drago L. 2014. Photodynamic antibacterial and antibiofilm activity of RLP068/CI against *Staphylococcus aureus* and *Pseudomonas aeruginosa* forming biofilms on prosthetic material. *Int J Antimicrob Agents* 44:47–55. <https://doi.org/10.1016/j.ijantimicag.2014.03.012>.
 83. Wood TL, Gong T, Zhu L, Miller J, Miller DS, Yin B, Wood TK. 2018. Rhamnolipids from *Pseudomonas aeruginosa* disperse the biofilms of sulfate-reducing bacteria. *NPJ Biofilms Microbiomes* 4:22–28. <https://doi.org/10.1038/s41522-018-0066-1>.
 84. Faoro V, Stanta G. 2011. Sample preparation and in gel tryptic digestion for mass spectrometry experiments, p 289–291. *In* Stanta G (ed), *Guidelines for molecular analysis in archive tissues*. Springer-Verlag, Berlin, Germany.
 85. Goldfarb D, Wang W, Major MB. 2016. MSAcquisitionSimulator: data-dependent acquisition simulator for LC-MS shotgun proteomics. *Bioinformatics* 32:1269–1271. <https://doi.org/10.1093/bioinformatics/btv745>.
 86. Chanukuppa V, Taware R, Taunk K, Chatterjee T, Sharma S, Somasundaram V, Rashid F, Malakar D, Santra MK, Rapole S. 2021. Proteomic alterations in multiple myeloma: a comprehensive study using bone marrow interstitial fluid and serum samples. *Front Oncol* 10:566804. <https://doi.org/10.3389/fonc.2020.566804>.
 87. Ludwig C, Gillet L, Rosenberger G, Amon S, Collins BC, Aebersold R. 2018. Data-independent acquisition-based SWATH-MS for quantitative proteomics: a tutorial. *Mol Syst Biol* 14:e8126. <https://doi.org/10.15252/msb.20178126>.
 88. Kumar B, Dey AK, Saha S, Singh AK, Kshetrapal P, Wadhwa N, Thiruvengadam R, Desiraju BK, Bhatnagar S, Salunke DM, Rashid F, Malakar D, Maiti TK, GARBH-Ini Study Group. 2021. Dynamic alteration in the vaginal secretory proteome across the early and mid-trimesters of pregnancy. *J Proteome Res* 20:1190–1205. <https://doi.org/10.1021/acs.jproteome.0c00433>.
 89. Gene Ontology Consortium. 2019. The gene ontology resource: 20 years and still GOing strong. *Nucleic Acids Res* 47:D330–D338. <https://doi.org/10.1093/nar/gky1055>.
 90. Otasek D, Morris JH, Bouças J, Pico AR, Demchak B. 2019. Cytoscape automation: empowering workflow-based network analysis. *Genome Biol* 20:185. <https://doi.org/10.1186/s13059-019-1758-4>.